Analysis of the Cooling Performance of a Cylindrical Hole Designed for the Suction Side of the LS89 Vane under Transitional Conditions

ANALYSIS OF THE COOLING PERFORMANCE OF A CYLINDRICAL HOLE DESIGNED FOR THE SUCTION SIDE OF THE LS89 VANE UNDER TRANSITIONAL CONDITIONS

N. Rosafio - A. Bruno - S. Salvadori[1] *- D. Misul - M. Baratta*

Dipartimento Energia (DENERG), Politecnico di Torino, Corso Duca degli Abruzzi, 24 - 10129 Torino, Italia

ABSTRACT

Thermal performance of film cooling in a transonic high-pressure vane is studied by means of two different turbulence modelling strategies: the γ-Re_Θ transition model and the fully turbulent k-ω SST model. Selected test case is the LS89 vane, appropriately modified to include a cylindrical film cooling device. The MUR237 transonic configuration is selected as representative of highly loaded vanes without shocks, with transonic Mach number over the suction side. The specifically designed cooling system is based on the non-dimensional geometrical and operating conditions of the high-pressure transonic MT1 cooled vane. Transition model constants are initially tuned to match the available experimental data for the original (uncooled) configuration. Eventually, results obtained with both models are compared with each other for several jet conditions, showing non-negligible influence of turbulence modelling on flow distribution and mixing between coolant and main-flow.

KEYWORDS

Turbomachinery, Heat Transfer, Film Cooling, Computational Fluid Dynamics, Transition Modelling

NOMENCLATURE

C	Chord
C_D	Discharge Coefficient
h_f	Iso-Energetic Heat Transfer Coefficient
L	Film Cooling Hole Length
M	Blowing Ratio
$NHFR$	Net Heat Flux Reduction
P	Pitch
$\dot{q}_0$	Heat flux, uncooled case
$\dot{q}_f$	Heat flux, film cooled case
S	Curvilinear Abscissa
T_{aw}	Adiabatic Wall Temperature
$T_{rec,m}$	Main-Flow Recovery Temperature
α	Film Cooling Hole Angle
η	Adiabatic Film Cooling Effectiveness
Θ	Non-Dimensional Wall Temperature

[1]Contact author: simone.salvadori@polito.it

INTRODUCTION

The need to increase gas turbine engine efficiency to have beneficial effects on specific fuel consumption and emissions, leads gas turbine manufacturers towards higher and higher operating temperatures (Horlock (2000), Bontempo & Manna (2019) and Baratta et al. (2020)). Film cooling is a well-established technology adopted to relieve stressed components from the thermal loads due to hot gas entering the high-pressure turbine stage. Such technology relies on a relatively low temperature flow, extracted from the last stages of the compressor, which shields vanes and blades surfaces from the hot main-flow.

Current knowledge about film cooling technology is based on countless studies and publications that give manufacturers and researchers a great amount of relevant information. Among the most relevant studies about cylindrical holes without internal cooling cross-flow, which is the topic of interest of the present work, it is worth mentioning the work of Fric & Roshko (1994) where the flow structures generated by the main-flow/coolant interaction are clearly described. Baldauf et al. (1999*b*) and Baldauf et al. (1999*a*) provided a comprehensive amount of high resolution measurements of effectiveness and heat transfer under several engine-relevant working conditions. Walters & Leylek (1997) clearly described velocity magnitude maps for cylindrical holes for several blowing ratios and geometrical configurations. Schwarz & Goldstein (1989) and Schwarz et al. (1991) gave important information about the performance of cooling arrays on curved surfaces. Ahlfeld et al. (2018) and Salvadori et al. (2019) gave information about the impact of manufacturing uncertainty and turbulence modelling on film cooling effectiveness in transonic and supersonic regimes.

However, there are still aspects that can be analyzed especially considering the increased accuracy of numerical methods for the analysis of boundary layer development and transition to turbulence. In the present paper, a high-pressure vane has been numerically investigated to capture the impact of a transitional boundary layer on the performance of a cylindrical film cooling hole. That topic is rarely investigated due to the fact that high-pressure turbine vanes are usually equipped with a showerhead configuration at leading edge that triggers boundary layer transition, thus generating a turbulent boundary layer on the rear suction side. Nonetheless, a thorough analysis of such configuration would help understanding some basic phenomena that occur in the main-flow/coolant interaction region in transitional regime, aiming at deducing useful information for future applications.

The LS89 test case has been selected as representative of a high-pressure vane in transonic conditions, and a cylindrical film cooling device has been designed based on the non-dimensional parameters of the experimentally analyzed MT1 cooled vane (Insinna et al. (2014)). The original configuration has been experimentally analyzed by Arts et al. (1990) thus providing information for various Reynolds numbers (ranging from $5\text{x}10^5$ to $2\text{x}10^6$), exit Mach numbers and turbulence levels. The relevance of the LS89 vane in gas turbine research field is proven by the enduring streak of publications, which involves the study of intermittency effect (Dupuy et al. (2020)) and the analysis of the impact of entropy waves on wall heat transfer (Hu et al. (2020)). The selected γ-Re_Θ transition model is tuned considering the MUR237 configuration, then the cooling geometry is designed and characterized using both fully turbulent and transition models. Relevant parameters like discharge coefficient, adiabatic effectiveness and Net Heat Flux Reduction are compared, thus demonstrating the non-negligible effect associated with an incoming transitional boundary layer on cooling performance.

TEST CASE DESCRIPTION

The LS89 is a transonic high-pressure vane instrumented for aerodynamic and thermal measurements, investigated at the Von Karman Institute for Fluid Dynamics. The vane was studied for several operating conditions, spanning different values of total inlet temperature and pressure and free-stream turbulence intensities. For the present numerical campaign the set of boundary conditions of the MUR237 case has been chosen (Arts et al. (1990)). This represents a transonic case, without shocks, where the outlet Mach number is 0.775. A film cooled configuration of the vane has been designed including a film cooling hole on the suction side. In order to guarantee realistic geometrical and operating conditions, a fully scaled up model of the cooling solution adopted on the high pressure MT1 vane has been designed (Insinna et al. (2014)) (Fig. 1). LS89 cooled configuration features the same pitch/diameter, length/diameter and coolant to main-flow total temperature ratios of the MT1 cooled vane. A novelty with respect to typical modelling of film cooling geometries is the design of a fillet radius at the junction between the film cooling channel, the vane surface and the plenum wall. There are two main reasons for this choice. On one hand, sharp edges are not realizable in practice because of wear and manufacturing uncertainties. Secondly, sharp edges are critical in the mesh generation routine due to the vanishing radius of curvature. Hence, a fillet radius allows to obtain a better spatial discretization of the domain, necessary to predict the curvature of the flow from the coolant inlet into the film cooling channel (Adami et al. (2002)). The fillet radius was designed according to the uncertainty quantification studies carried out by Montomoli et al. (2011) who individuated the best fillet radius to reproduce experimental data in compressible regime. Further details about the geometry, the boundary conditions of the cooled vane and the reference experimental test case are reported in Tab. 1.

Total Inlet Temperature [K]	417.3
Total Inlet Pressure [bar]	1.753
Static Outlet Pressure [bar]	1.179
Outlet Mach Number [-]	0.775
Turbulence Intensity [%]	6
Wall Temperature [K]	299.85

(a) **MUR237 conditions**

Coolant Total Temperature [K]	269.16
Coolant Total Pressure [bar]	Variable
P/D [-]	3
L/D [-]	5.4
R/D [-]	0.05
α [°]	30

(b) **Cooled vane characteristics**

Table 1: **Experimental and numerical campaigns conditions**

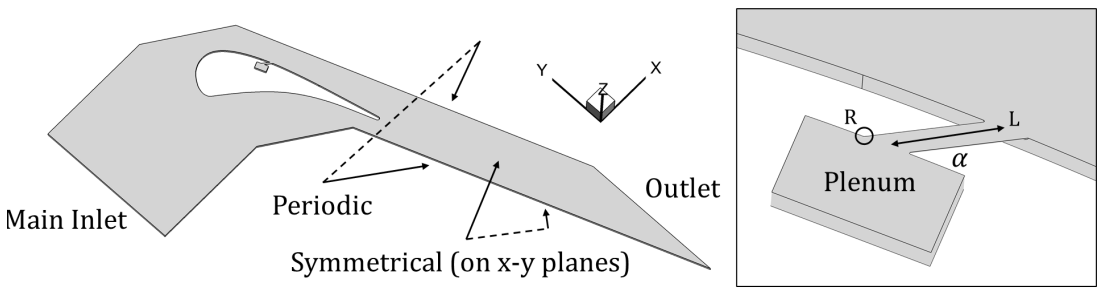

Figure 1: **Cooled LS89 computational domain**

NUMERICAL METHODOLOGY

The numerical campaign was run through the commercial software Star-CCM+. The 2-equation k-ω SST turbulence model (Menter (1994)) in combination with the γ-Re_Θ transition model (Menter et al. (2004)) were used to model turbulence and natural transition of the boundary layer over the suction side of the vane. A second set of simulations was run without transition modelling to investigate the relative effect of boundary layer transition on the thermal performance of film cooling, when the hole is positioned in a transitional region. Second order spatial discretization was implemented for convective terms of flow and turbulence equations. Hybrid Gauss-Green Least-Square method was used for the reconstruction of gradients.

The numerical methodology was validated in a test case that reproduces a 2D version of the uncooled LS89 vane. Numerical results were compared with available experimental data and transition model constants were tuned to correctly capture the main-flow boundary layer development over the suction side of the original vane. The results of the tuning procedure are presented in Fig. 2, where experimental values of the MUR237 case are plotted along with the numerical results obtained with the original transition and the fully turbulent models.

The fully turbulent model is inherently incapable of reconstructing the transitional boundary layer over the suction side of the blade. As a matter of fact, after a slight decrease of the heat transfer coefficient after the stagnation point, a turbulent boundary layer is predicted by the model. Experimental results are not correctly captured on the pressure side either. As far as the transition model is regarded, it is evident how the original constants fail to capture the experimental transition length. Improved predicting capability was obtained on the vane suction side through the tuning procedure, which allows to correctly capture the trend of variation of the heat transfer coefficient. It must be said that, the tuned constants do not predict correctly the heat transfer coefficient values over the pressure side, which are correctly captured through the original model constants though. This behaviour was expected since the diffusion constant of Re_Θ (σ_θ) and the production/destruction constant of γ (ca_2) were modified, affecting the model behaviour on both the pressure side and the suction side. The original values for σ_θ and ca_2 are respectively equal to 10 and 0.03. The tuned values are equal to 2.2 and 0.5. Despite this, since the solid region was not simulated, the predicting capability of the model over the pressure side does not affect the numerical results over suction side, which represents the main focus of the present investigation.

Regarding aerodynamics, the experimental pressure distribution over the vane of the MUR237 test case is not available in the literature. For this reason the numerical pressure distribution (black line in Fig. 3) is compared with the experimental data available for Ma_2=0.875. Experimental data are met over the pressure side of the blade. The underestimation of the isentropic Mach number over the suction side is addressed to the higher outlet Mach number of the experimental campaign, which generates a greater acceleration of the flow over the section side.

Mesh generation

A mesh sensitivity analysis was performed on the cooled configuration. The boundary conditions imposed for the mesh sensitivity analysis represent the case of M=1. The mesh was generated by means of Centaur^{TM}, a commercial hybrid mesh generator by Centaursoft. Prismatic and tetrahedral elements were combined into hybrid meshes. Assuming the symmetry of the flow about the center plane of the cooling hole and about the half-pitch plane, meshes have been generated on half geometry. Symmetric conditions have been implemented over the half-pitch plane and center plane of the cooled vane.

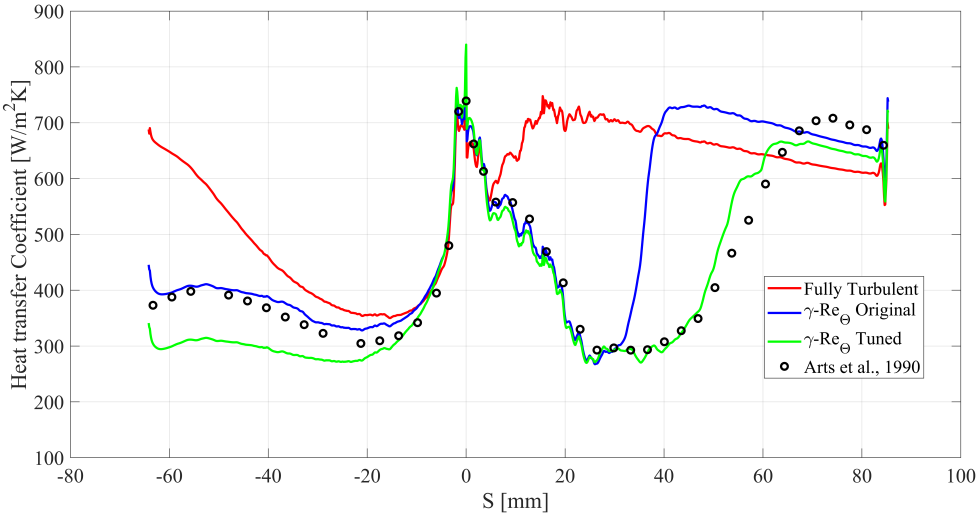

Figure 2: **Heat transfer coefficient distribution**

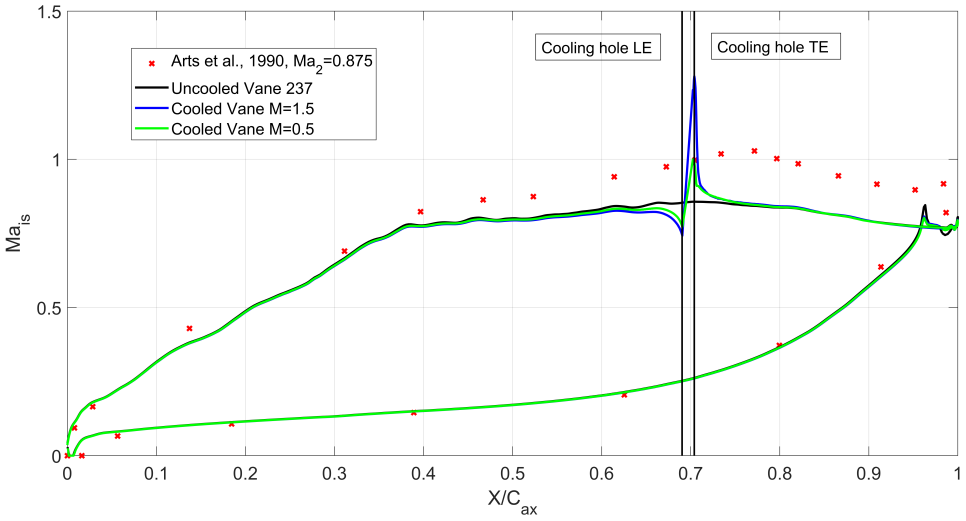

Figure 3: **Isentropic Mach number distribution**

The mesh sensitivity study has been carried out by generating 4 different meshes. The surface and volume density of elements was increased from a coarse to a fine level both in the region of interaction between coolant and main-flow and downstream of the coolant exit section. Both global quantities and local maps were compared to establish the sensitivity of the results to the mesh. The variations of the monitored global quantities were always below $<1\%$.

In order to appreciate the variation of local quantities, isolevels of temperature over the cooled region are shown in Fig. 4 for the adiabatic case. Some minor differences in coolant distribution can be noticed for coarser meshes, whereas the solution becomes grid independent at 3.6M elements. This mesh has been selected to perform the final numerical campaign. The details of the grid at the Leading Edge, Trailing Edge and in the coolant/main-flow interaction

region are shown in Fig. 5.

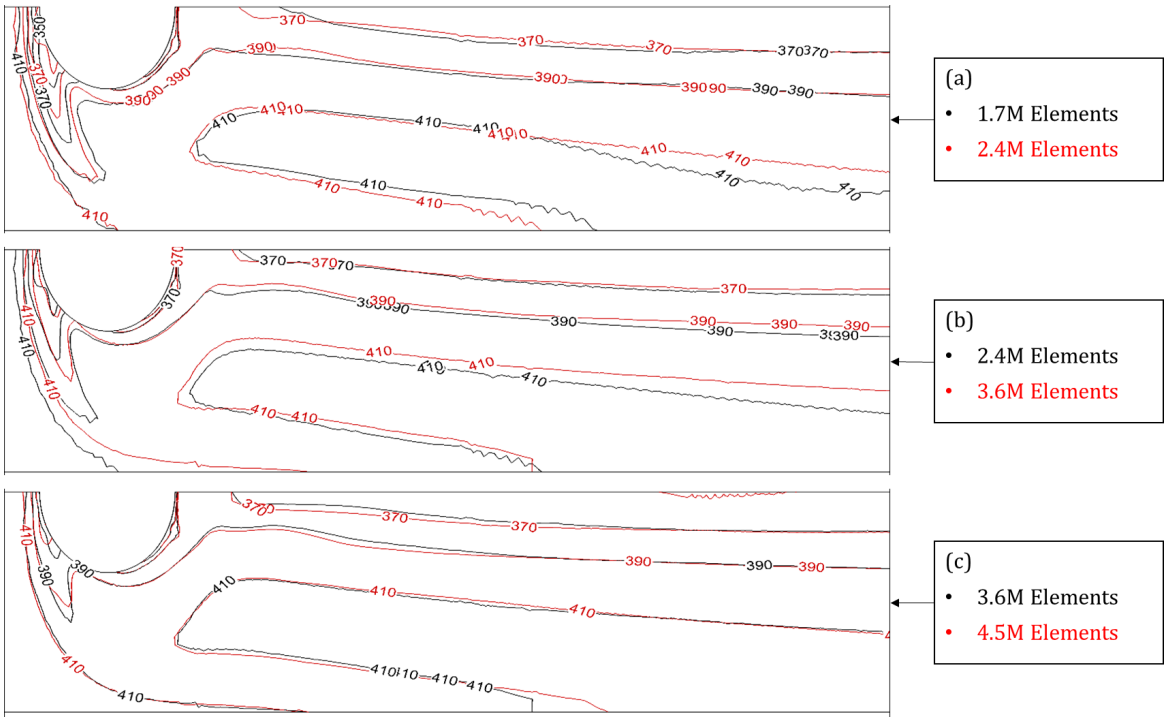

Figure 4: **Mesh sensitivity results - Temperature [K] iso-lines**

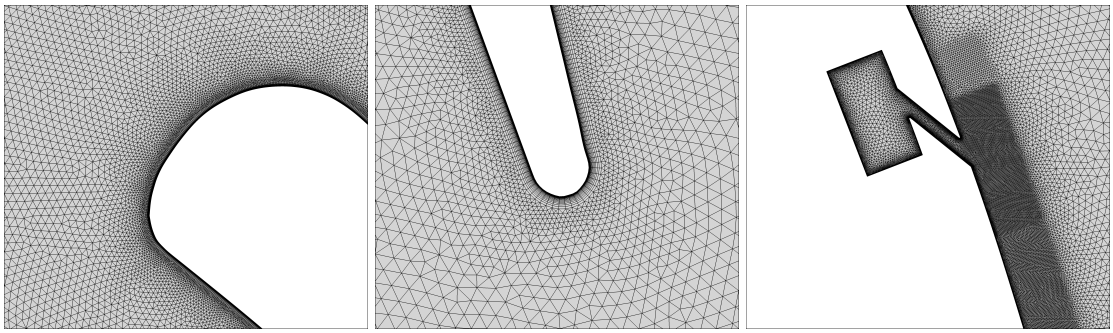

(a) **Leading Edge** (b) **Trailing Edge** (c) **Jet exit region**

Figure 5: **Mesh details**

RESULTS

In the present section, the results of the numerical campaign are reported. The aerodynamics, in terms of discharge coefficient and pressure distribution, is discussed first. The thermal performance of the cooling technology is assessed next by means of adiabatic effectiveness and Net Heat Flux Reduction. The main differences between the transitional approach and fully turbulent modelling are emphasised.

Aerodynamics

The discharge coefficient (Eq. 1), compares the actual mass flow rate delivered through the hole with an ideal one. The film cooling hole cross section is set as the reference area and the ideal mass flow rate is computed considering the limiting case of isentropic expansion from coolant total inlet conditions to the static pressure at the cooling hole discharge section.

$$C_D = \frac{\dot{m}_c}{p_{0c}\left(\frac{p_m}{p_{0c}}\right)^{\frac{\gamma+1}{2\gamma}}\left(\frac{2\gamma}{(\gamma-1)RT_{0c}}\left(\left(\frac{p_{0c}}{p_m}\right)^{\frac{\gamma-1}{\gamma}}-1\right)\right)^{0.5}\pi\frac{D^2}{4}} \tag{1}$$

Fig. 6 shows the discharge coefficient plotted against the pressure ratio. 'Circle' markers highlight the points where the investigated values of M (0.5 - 0.75 - 1 - 1.5) are met. The numerical results are tested against experimental values of a linear test case (Ochs et al. (2007)) which features a Mach number upstream of the coolant jet equal to 0.8. This value is comparable with the Mach reached over the suction side of the investigated cooled vane. As shown in the work by Salvadori et al. (2013), discrepancies between numerical predictions and experimental values are typically addressed to bad/lack of modelling of the coolant plenum. In this case, numerical results are in close accordance with experimental values which confirms a fair numerical modelling of the inlet plenum.

In film cooling applications, coolant jets modify the pressure distribution over the vane profile. A high pressure region is found at the leading edge of the coolant exit section, which is due to the blockage effect of the jet on the main-flow. At the trailing edge, low pressure is found, due to jet penetration into the main-flow. Pressure distributions, via isentropic Mach numbers, are shown in Fig. 3 for the limiting values of the blowing ratio along with the uncooled case. The higher the blowing ratio, the larger are the values of Ma_{is} at the leading edge and the lower are the values at the trailing edge of the hole.

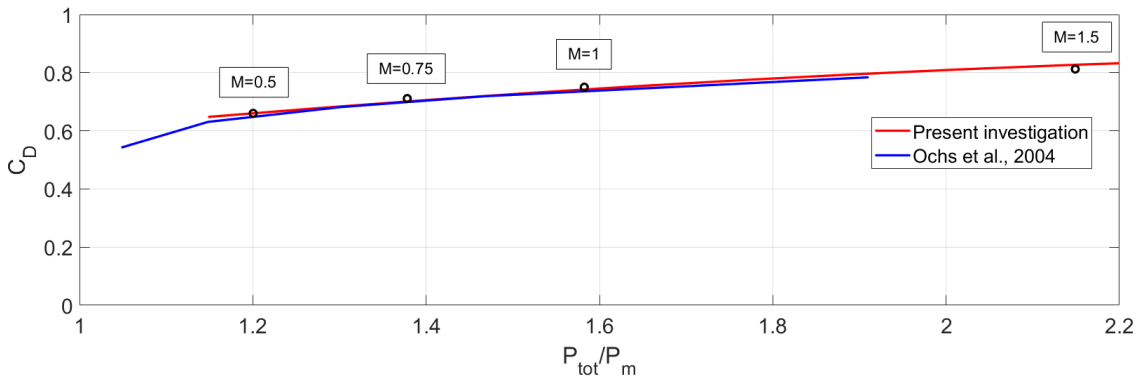

Figure 6: **Discharge Coefficient**

Heat transfer

As far as the thermal performance of the cooling technology is considered, results are presented in terms of adiabatic effectiveness (η) and Net Heat Flux Reduction (NHFR) which are respectively defined by Eq. 2 and 3.

$$\eta = \frac{T_{aw} - T_{rec,m}}{T_{0c} - T_{rec,m}} \tag{2}$$

$$NHFR = \frac{\dot{q}_0 - \dot{q}_f}{\dot{q}_0} \tag{3}$$

where:

$$T_{rec,m} = T_{0m} \frac{1 + Pr^{0.33} \frac{\gamma-1}{2} Ma_{is}^2}{1 + \frac{\gamma-1}{2} Ma_{is}^2} \tag{4}$$

The heat flux for the cooled vane can be computed through Eq. 5:

$$\dot{q}_f = h_f \left(T_{aw} - T_w\right) = h(\Theta)(T_{rec,m} - T_w) \tag{5}$$

where Θ is defined as:

$$\Theta = \frac{T_{0c} - T_{rec,m}}{T_w - T_{rec,m}} \tag{6}$$

The thorough thermal characterization of the cooling technology was carried out varying the thermal condition imposed over the profile. Adiabatic effectiveness maps are obtained by imposing adiabatic conditions at the wall. On the other hand, the computation of the heat transfer coefficient requires isothermal conditions over the profile. The results are then combined to calculate the NHFR.

Adiabatic Effectiveness

Fig.7 shows the maps of η at various blowing ratios for the fully turbulent model and the transition model, respectively. The first effect of transition modelling on the distribution of the adiabatic effectiveness is the back-flow originating at the leading edge of the exit section. This behaviour is not matched by the results obtained with fully turbulent modelling and the main reason is found in the main-flow boundary layer velocity distribution. A fully turbulent boundary layer is more energetic than the transitional one and can withstand the adverse pressure gradient created by the ejection of the coolant in the main-flow (as shown in Fig. 8). This inhibits back-flow, resulting in a value of η before the coolant injection equal to 0. The back-flow has a twofold effect. Besides contributing to the cooling of the portion of the blade before the leading edge, it is convected by the hot gas, creating cold wings around the coolant exit section. Lateral transport of cold flow in the span-wise direction of the blade is present as well, even though it is evident only for low values of the blowing ratio.

The second (minor) difference between the two turbulence modelling approaches shows up after the coolant exit section. As a matter of fact, for all investigated blowing ratios, the value of η in the proximity of the exit section is higher when transition is modelled. In order to appreciate this behaviour, laterally averaged adiabatic effectiveness has been plotted against the non-dimensional curvilinear abscissa in Fig. 9. In this case, the origin of the reference frame is the center of the cooling hole exit section. At all blowing ratios, transition model predicts higher values in the proximity of the hole. Depending on the cold flow penetration, the difference can be as high as 0.15 for M=0.5. Both models tend to recover the same trend moving downstream towards the blade trailing edge. Actually, a slight difference in lateral spreading in the coolant between the two models has been found, but it is almost negligible as shown in Fig. 7.

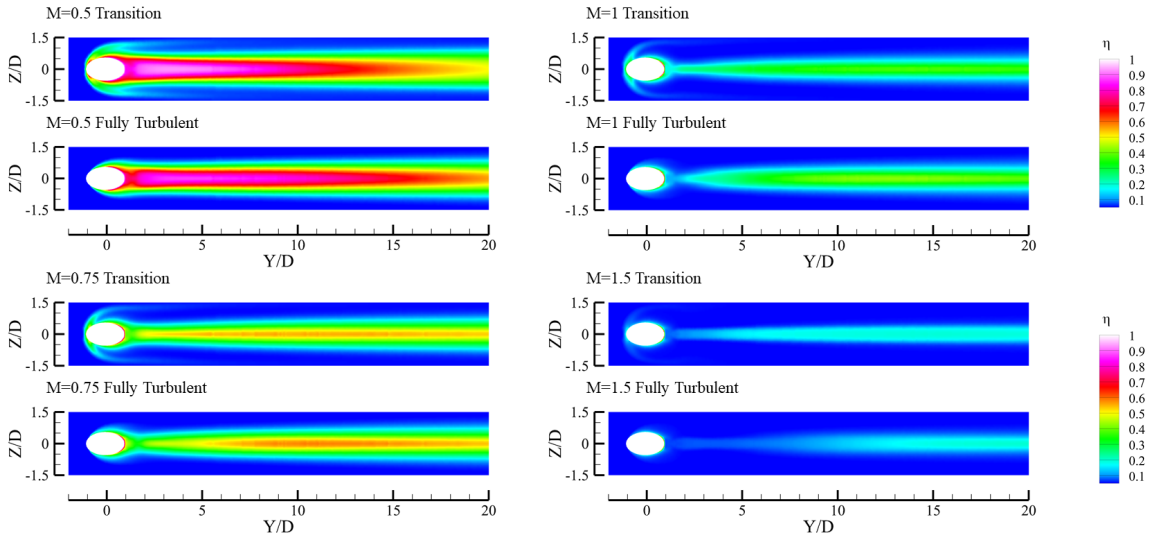

Figure 7: **Adiabatic effectiveness**

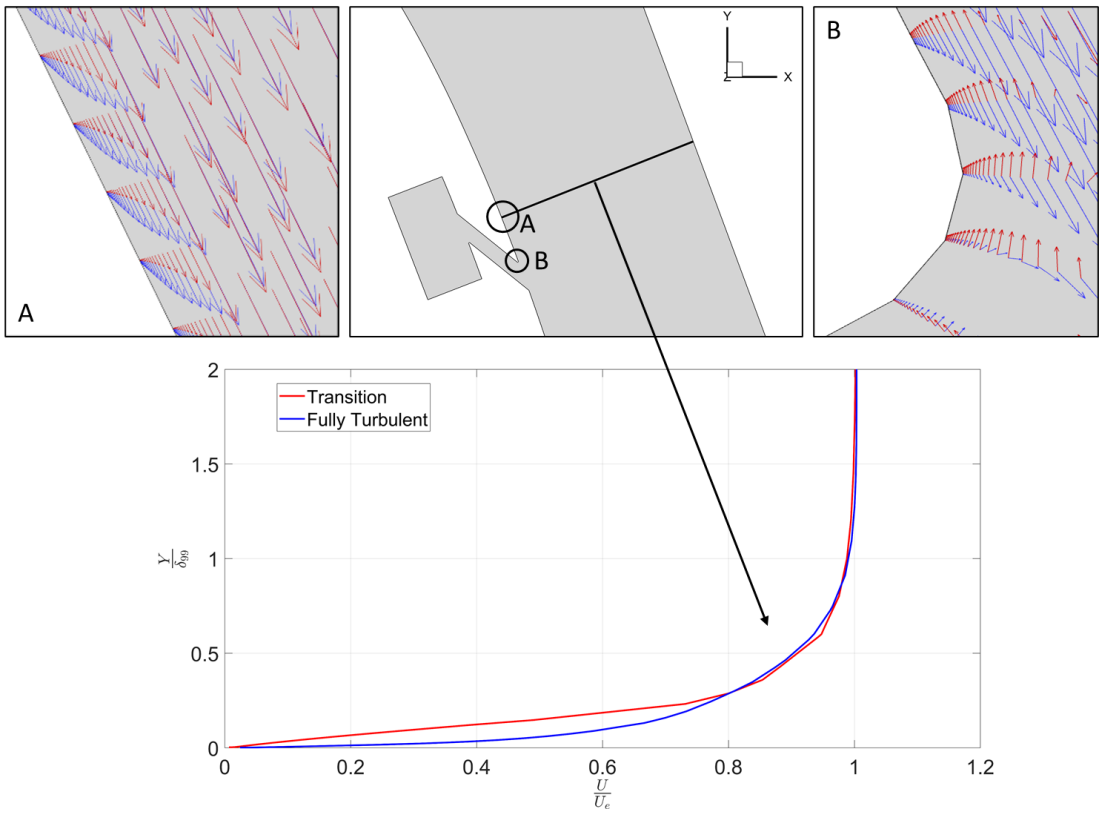

Figure 8: **SS velocity profile and back-flow: Fully turbulent (blue), Transition model (red)**

Net Heat Flux Reduction

NHFR maps are reported in Fig. 10. In general, NHFR maps show positive values close to the center-line, where coolant shields the surface from the hot gas. Locally low values (down to -3) of the NHFR are found in the regions of interaction between the main-flow and the coolant

which are associated with high values of the heat transfer coefficient for the cooled vane. Once the interaction is smeared out by viscous and turbulent stresses, positive values of NHFR are found. In order to better visualize trends in NHFR, laterally averaged values are presented in Fig. 9 as well. Referring to the transition model predictions, for low distances from coolant jet position (S/D$<$10), a lower blowing ratio yields higher values of NHFR$_{lat}$. The maximum value (0.4) is reached for M=0.5. This is mainly attributable to the better coverage of the surface by the coolant as shown by the adiabatic effectiveness distributions. On the other hand, for S/D$>$16, M=0.5 case features the lowest heat flux reduction, whereas the highest ones are obtained with the intermediate blowing ratios. The NHFR is as high as 0.6 for M=0.75 and M=1, in this region. As it was expected, the NHFR obtained with a fully turbulent model is always lower than the corresponding transitional case. The highest difference ($\approx$0.6) is noted at M=1.5. Moreover, for S/D$>$14, each of the fully turbulent cases features a worse thermal performance than any of the cases modelled with transition.

According to the authors, the main cause of this behaviour is the overestimation of turbulence levels when the fully turbulent model is adopted. In Fig. 11, streamlines coloured by non-dimensional turbulent kinetic energy of the case M=1 are plotted covering the downstream and upstream regions of the coolant exit section. Streamlines are seeded in the hot gas boundary layer, before the interaction with the coolant for both turbulence models. Looking at the streamlines, it can be observed that the hot gas convected downstream of the coolant exit section is responsible for the increase of turbulent kinetic energy. Furthermore, shear stresses addressed to the interaction between coolant and hot gas contribute to turbulence production. Comparing the results obtained with both turbulence modelling approaches, it is visible that the interaction between hot and cold gas generates similar levels of turbulence for the two turbulence models. This mechanism mainly affects the turbulence distribution, hence the mixing, at the coolant/hot gas interface. On the other hand, the convected turbulence modifies the turbulence distribution in the boundary layer. When the fully turbulent model is adopted, high values of turbulent kinetic energy result from the inability to reproduce the transitional boundary layer upstream of the coolant ejection. The convection of this flow downstream, promotes heat flux at the wall which explains the low values of NHFR predicted by the fully turbulent model.

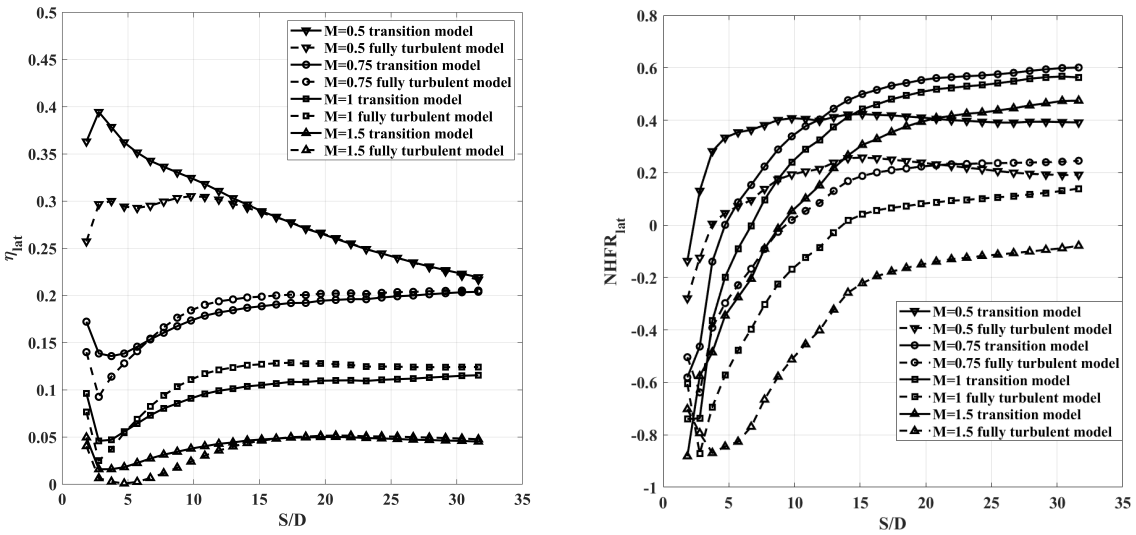

Figure 9: **Laterally averaged results**

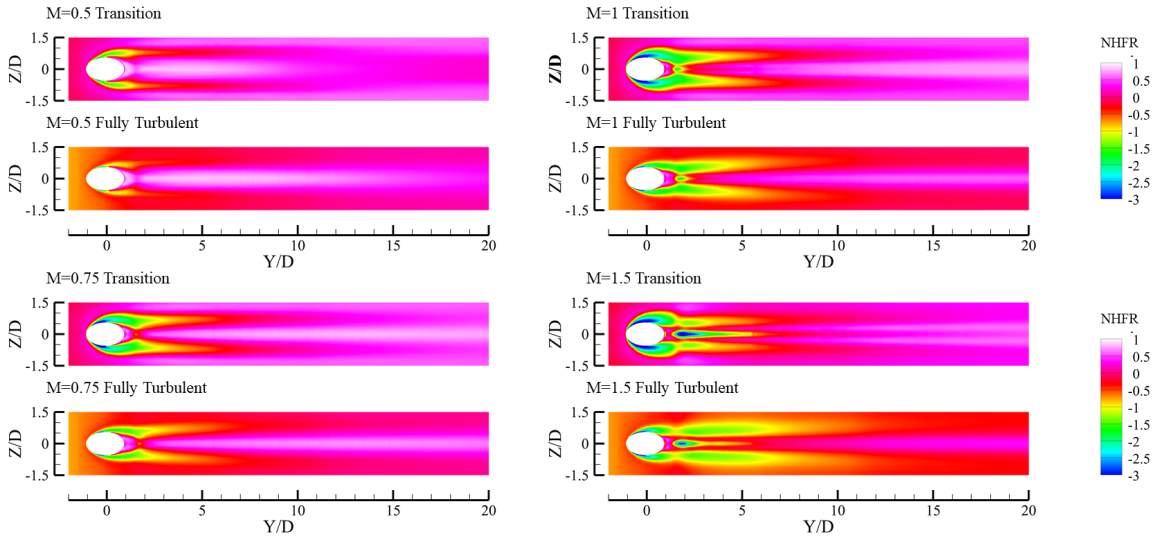

Figure 10: **Net Heat Flux Reduction**

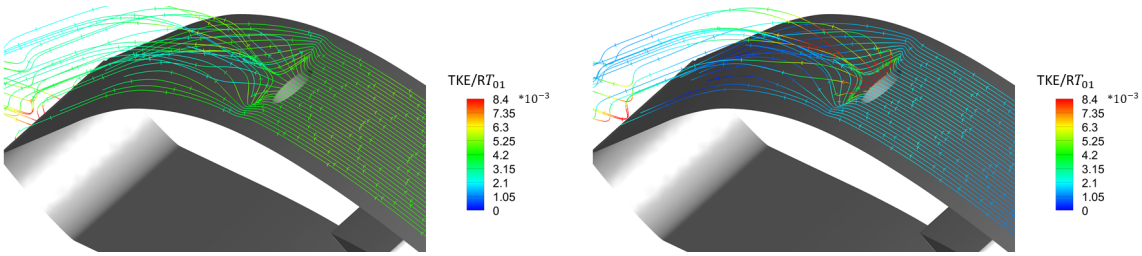

(a) **Fully turbulent model** (b) **Transition model**

Figure 11: **TKE over main-flow streamlines**

CONCLUSIONS

In this work, a film cooling solution for a high-pressure vane in transonic regime has been designed and assessed at various jet conditions. The numerical campaign was conducted adopting two different approaches for turbulence modelling: k-ω SST with and without the γ-Re$_\Theta$ transition model. At first, transition model constants have been tuned in order to correctly predict the development of the main-flow boundary layer in the region of interaction with the coolant. Then the aerodynamics and the thermal results obtained with both models have been compared for 4 different blowing ratios.

The first outcome of the present numerical campaign is that the prediction of the state of the boundary layer retains a high effect on the evaluation of the thermal performance of film cooling solution. Transitional boundary layers might not withstand high-pressure regions at the coolant exit section, generating back-flow and lateral transport which modifies the distribution of cold flow over the cooled surface. This effect is highly dependent on jet conditions and becomes almost negligible at high blowing ratios (M=1.5). In despite of this, predicted η trends are similar except in the proximity of the jet exit section. where coolant coverage is better when transition is modelled.

Concerning NHFR, the thermal performance predicted by the transition model is better for all the investigated jet conditions. It was found that the main reason for the low values predicted by the fully turbulent model can be addressed to the overestimation of turbulent kinetic energy over the transitional region of the suction side, which enhances the downstream heat transfer at the solid wall.

ACKNOWLEDGEMENTS

Computational resources were provided by HPC@POLITO (http://hpc.polito.it).

REFERENCES

Adami, P., Martelli, F., Montomoli, F. & Saumweber, C. (2002), 'Numerical Investigation of Internal Crossflow Film Cooling'. doi: 10.1115/GT2002-30171.

Ahlfeld, R., Montomoli, F., Carnevale, M. & Salvadori, S. (2018), 'Autonomous Uncertainty Quantification for Discontinuous Models Using Multivariate Padé Approximations', *Journal of Turbomachinery* **140**(4). 041004, doi: 10.1115/1.4038826.

Arts, T., de Rouvroit, M. L., Rutherford, A. W. & Von Karman Institute for Fluid Dynamics (1990), 'Aero-thermal Investigation of a Highly Loaded Transonic Linear Turbine Guide Vane Cascade: A Test Case for Inviscid and Viscous Flow Computations'.

Baldauf, S., Schulz, A. & Wittig, S. (1999*a*), 'High-Resolution Measurements of Local Effectiveness From Discrete Hole Film Cooling ', *Journal of Turbomachinery* **123**(4), 758–765. doi: 10.1115/1.1371778.

Baldauf, S., Schulz, A. & Wittig, S. (1999*b*), 'High-Resolution Measurements of Local Heat Transfer Coefficients From Discrete Hole Film Cooling ', *Journal of Turbomachinery* **123**(4), 749–757. doi: 10.1115/1.1387245.

Baratta, M., Cardile, F., Misul, D., Rosafio, N., Salvadori, S., Forno, L. & Toppino, M. (2020), 'Redesign of the TG20 Heavy-Duty Gas Turbine to Increase Turbine Inlet Temperature and Global Efficiency', *Proceedings of the ASME Turbo Expo 2020* . Virtual Conference, September 21-25.

Bontempo, R. & Manna, M. (2019), 'Work and Efficiency Optimization of Advanced Gas Turbine Cycles', *Energy Conversion and Management* **195**, 1255 – 1279. doi: 10.1016/j.enconman.2019.03.087.

Dupuy, D., Gicquel, L., Odier, N., Duchaine, F. & Arts, T. (2020), 'Analysis of the effect of intermittency in a high-pressure turbine blade', *Physics of Fluids* **32**(9), 095101. doi: 10.1063/5.0018679.

Fric, T. F. & Roshko, A. (1994), 'Vortical Structure in the Wake of a Transverse Jet', *Journal of Fluid Mechanics* **279**, 1–47. doi: 10.1017/S0022112094003800.

Horlock, J. H. (2000), 'The Basic Thermodynamics of Turbine Cooling ', *Journal of Turbomachinery* **123**(3), 583–592. doi: 10.1115/1.1370156.

Hu, K., Yuanqi, F., Zheng, Y., Wang, G. & Moreau, S. (2020), 'Numerical Investigation of Influence of Entropy Wave on the Acoustic and Wall Heat Transfer Characteristics of a High-Pressure Turbine Guide Vane', *Acoustics* **2**, 524–538. doi: 10.3390/acoustics2030028.

Insinna, M., Griffini, D., Salvadori, S. & Martelli, F. (2014), 'Film Cooling Performance in a Transonic High-pressure Vane: Decoupled Simulation and Conjugate Heat Transfer Analysis', *Energy Procedia* **45**, 1126 – 1135. ATI 2013 - 68th Conference of the Italian Thermal Machines Engineering Association, doi: 10.1016/j.egypro.2014.01.118.

Menter, F. R. (1994), 'Two-Equation Eddy-Viscosity Turbulence Models or Engineering Applications', *AIAA Journal* **32**(8), 1598–1605. doi: 10.2514/3.12149.

Menter, F. R., Langtry, R. B., Likki, S. R., Suzen, Y. B., Huang, P. G. & Völker, S. (2004), 'A Correlation-Based Transition Model Using Local Variables-Part I: Model Formulation', *Journal of Turbomachinery* **128**(3), 413–422. doi: 10.1115/1.2184352.

Montomoli, F., Massini, M., Salvadori, S. & Martelli, F. (2011), 'Geometrical Uncertainty and Film Cooling: Fillet Radii', *Journal of Turbomachinery* **134**(1). 011019, doi: 10.1115/1.4003287.

Ochs, M., Schulz, A. & Bauer, H. J. (2007), 'Report on Tests with Steady Shocks'. Universität Karlsruhe, Institut fuer Thermische Stroemungsmachinen, TATEF 2, Contract No. AST3-CT-2004-502924.

Salvadori, S., Carnevale, M., Fanciulli, A. & Montomoli, F. (2019), 'Uncertainty Quantification of Non-Dimensional Parameters for a Film Cooling Configuration in Supersonic Conditions', *Fluids* **4**, 155. doi: 10.3390/fluids4030155.

Salvadori, S., Montomoli, F. & Martelli, F. (2013), 'Film cooling performance in supersonic flows: Effect of shock impingement', *Proceedings of the Institution of Mechanical Engineers Part A Journal of Power and Energy* **227**, 295–305. doi: 10.1177/0957650912474444.

Schwarz, S. G. & Goldstein, R. J. (1989), 'The Two-Dimensional Behavior of Film Cooling Jets on Concave Surfaces', *Journal of Turbomachinery* **111**(2), 124–130. doi: 10.1115/1.3262246.

Schwarz, S. G., Goldstein, R. J. & Eckert, E. R. G. (1991), 'The Influence of Curvature on Film Cooling Performance', *Journal of Turbomachinery* **113**(3), 472–478. doi: 10.1115/1.2927898.

Walters, D. K. & Leylek, J. H. (1997), 'A Detailed Analysis of Film-Cooling Physics: Part I-Streamwise Injection With Cylindrical Holes ', *Journal of Turbomachinery* **122**(1), 102–112. doi: 10.1115/1.555433.